Available online at www.sciencedirect.com
ScienceDirect
Journal of Sound and Vibration 310 (2008) 1112–1127
JOURNAL OF SOUND AND VIBRATION
www.elsevier.com/locate/jsvi

Linear stochastic evaluation of tyre vibration due to tyre/road excitation

E. Rustighi[a,*], S.J. Elliott[a], S. Finnveden[b], K Gulyás[c], T. Mócsai[c], M. Danti[d]

[a]*Institute of Sound and Vibration Research, Southampton, UK*
[b]*MWL, Aeronautical and Vehicle Engineering, KTH, Stockholm, Sweden*
[c]*Budapest University of Technology and Economics, Budapest, Hungary*
[d]*Centro Ricerche FIAT, Torino, Italy*

Received 27 November 2006; received in revised form 21 August 2007; accepted 22 August 2007
Available online 17 October 2007

Abstract

Tyre/road interaction is recognised as the main source of interior and exterior noise for velocities over the 40 km/h. In this paper, a three-dimensional (3D) elemental approach has been adopted to predict the stochastic tyre vibration and hence the interior and exterior noise due to this kind of excitation. The road excitation has been modelled from the spectral density of a common road profile, supposing the road to be an isotropic surface. A linear Winkler bedding connects the 3D model of the tyre with the ground. The exterior noise has been evaluated by an elemental calculation of the radiation matrix of the tyre deformed by the static load on a concrete road. The noise inside the vehicle has also been calculated, using the transfer functions from the force transmitted to the hub and the noise inside the vehicle, which have been computed by a FEM model of a common car body. The simple formulation allows much quicker calculation than traditional nonlinear approaches, and appears to give results consistent with available measurements, although the effects of tyre rotation and of the nonlinearities in the contact model are yet to be quantified, and the method requires further experimental validation before practical application.

1. Introduction

Nowadays, because of the development of more silent vehicle power units, an important source of internal and external car noise is the interaction between tyre and road. For vehicle at normal driving conditions and speeds above 30–40 km/h the dominating external noise source is the sound generated by the tyre and road interaction [1]. Measurements on the noise generation mechanism show that there is a strong correlation between the radiated sound pressure and the vibrations of the tyre structure for frequency below approximately 1 kHz [2,3]. The recent design of lightweight vehicles has also increased the significance of the road/tyre noise inside the vehicle due to structure-borne vibration and acoustic radiation, affecting passenger comfort [4,5].

*Corresponding author. Tel.: +44 23 8059 2308; fax: +44 23 8059 3190.
E-mail address: er@isvr.soton.ac.uk (E. Rustighi).

0022-460X/$ - see front matter © 2007 Elsevier Ltd. All rights reserved.
doi:10.1016/j.jsv.2007.08.032

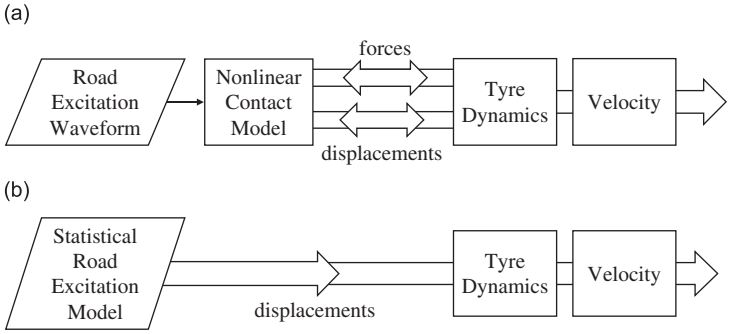

Fig. 1. Flow charts of nonlinear deterministic model (a) and linear stochastic model (b).

Road surface texture and tyre tread pattern create fluctuating forces that excite the tyre structure, producing vibrations. The interaction is generally nonlinear because of the time-varying nature of the contact area. Various models have been used to predict the noise generated by the interaction between a rolling tyre and the road surface [6]. These models can be classified in three categories: purely statistical models, e.g. Refs. [2,7], deterministic models, e.g. Refs. [8,9] and hybrids models, e.g. Ref. [10]. While deterministic models try to model the physical processes involved, statistical models try to find relationship among experimental measured data. Hybrid models use deterministic model in order to represent the contact mechanism and rely on statistical analysis in order to find data correlations.

Fig. 1(a) shows the flow chart for a deterministic nonlinear approach. The nonlinearity lies in the contact since the points of the tyre in contact with the ground change with time. Because of this an iterating calculation must be performed to find the forces and displacements at each time step. This procedure is numerically expensive although it does provide very detailed predictions.

In this paper, a three-dimensional (3D) linear model for the random excitation of a tyre's vibration and its subsequent sound radiation is presented. Fig. 1(b) shows the flow chart of this new approach illustrated in the paper. The model may be physically interpreted as assuming that the tyre is smooth and soft enough that the whole of the tyre surface in the contact patch connects with the road [11]. No iteration is needed in the calculation process, as shown in Fig. 1(b), reducing the numerical computation, although the major computational saving comes from being able to calculate the statistical properties of the response directly, rather than via long time domain simulations. The excitation of the tyre as it runs over a rough road is modelled as a random displacement distribution with a specified spatial correlation. This model is used to calculate the forces at a grid of discrete points in the contact patch. The spectral density matrix of radial velocities is then calculated from the structural mobility matrix for the dynamics of the tyre supported on the contact patch. The kinetic energy associated with the radial motion of the tyre and the sound power radiated by the tyre are subsequently calculated. The structure-borne sound inside the vehicle can then be calculated from the tyre's mechanical dynamic stiffness, which relates road displacement to hub forces, and from the vehicle's acoustic impedance matrix, that gives the relationship from hub forces to internal pressures. Rustighi and Elliott [12,13] already illustrated this methodology on a simpler two-dimensional (2D) model, and also investigated the feasibility of actively controlling the tyre vibrations. In this paper the method is extended using a more representative 3D model employing realistic tyre dynamics, sound radiation and sound transmission models.

2. The linear stochastic elemental approach

The 3D tyre model is assumed to be divided into N_T discrete elements, as shown in Fig. 2. The vector of complex radial velocities at the corners of each rectangular element, $\mathbf{v}_T$, are assumed to be related to the vector of all the complex forces acting on the elements, $\mathbf{f}_T$, via the matrix of structural mobilities for the free tyre suspended off the ground, $\mathbf{Y}_F$, so that

$$\mathbf{v}_T = \mathbf{Y}_F \mathbf{f}_T. \tag{1}$$

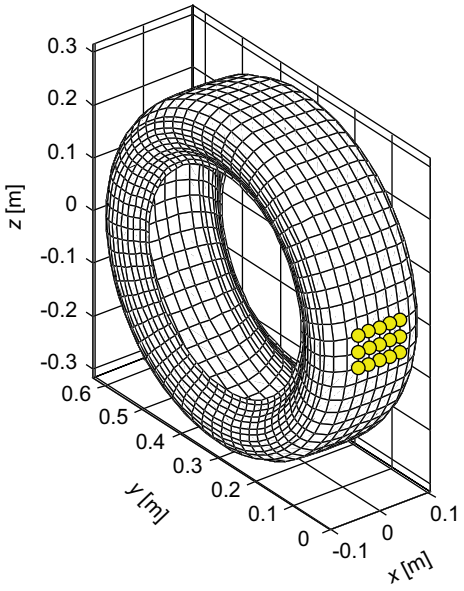

Fig. 2. Mesh used for the tyre model. The circles indicate the chosen contact points.

In this paper we assume the contact stiffness is generated only by a set of isolated, locally acting, springs, which is called a Winkler bedding [14,15]. A model will be used, assuming that all of the contact patch is in touch with the road at all times. Such an approximation would hold in the limiting case of a smooth soft tyre travelling over a road which is not too rough, such that the road displacement is small compared with the static compression of the tyre in the contact patch [11]. In the case where contact nonlinearity is important, it is possible that such behaviour in the contact patch could be taken into account by a modification of the excitation matrix. The confirmation of such an approximation and the definition of its range of validity are presently under investigation.

The interaction between the tyre tread and the rough road is modelled here by a bedding of N_C independent springs that connect each point on the road, with vertical displacement $\mathbf{d}$, to each point in the contact patch on the tyre, with vertical tyre displacement $\mathbf{w}$, which are assumed to be equal to the radial tyre displacements since the contact patch is usually small compared with the circumference. The tangential excitation due to friction has not been accounted for.

The force at all N_T points on the tyre is related to the difference between the road and tyre displacements by the linear equation

$$\mathbf{f}_T = \mathbf{K}_{TC}(\mathbf{d} - \mathbf{w}), \tag{2}$$

where $\mathbf{K}_{TC}$ is an $N_T \times N_C$ matrix describing the linear contact stiffness. In the case of a Winkler bedding, $\mathbf{K}_{TC}$ has N_C diagonal elements equal to the individual contact stiffnesses k_i, and the other elements are zero.

The displacement of the tyre in the contact patch caused by these forces is now written as

$$\mathbf{w} = \mathbf{C}_{CT}\mathbf{f}_T, \tag{3}$$

where $\mathbf{C}_{CT}$ is the $N_C \times N_T$ matrix of tyre compliances at the points in the contact patch. These compliances can be calculated as a subset of the mobilities in Eq. (1), divided by $j\omega$.

The vector of radial velocities for the tyre due to the road roughness can then be calculated from Eqs. (1)–(3), as

$$\mathbf{v}_T = \mathbf{T}\mathbf{d}, \tag{4}$$

where the overall transfer matrix, $\mathbf{T}$, is equal to $\mathbf{Y}_F[I + K_{TC}C_{CT}]^{-1}K_{TC}$.

The excitation of the tyre as it runs over a rough road is modelled as a random displacement distribution with a specified spatial correlation. If the contact patch is divided into a fine grid, the force distribution can be

approximated by a vector of forces acting at the elements defined by the grid. Each force will have a random time history, which can be assumed to be stationary, with its own autocorrelation function and a set of cross-correlation functions with the other forces acting in the contact patch.

The individual road displacement spectra are grouped together in an $N_C \times 1$ vector, $\mathbf{d}$, and the spectral density matrix of the road displacement is then defined to be [16]

$$\mathbf{S}_{dd} = E[\mathbf{d}\mathbf{d}^{\mathrm{H}}], \tag{5}$$

where E denotes the expectation operator and $(\cdot)^{\mathrm{H}}$ denotes the Hermitian, complex conjugate, transpose. The diagonal elements of $\mathbf{S}_{dd}$ correspond to the power spectral densities of each of the displacements, which will be assumed to be equal in this model, and the off-diagonal terms correspond to cross spectral densities between the displacement at different points.

Since the model is fully linear, the spectral density matrix of the tyre's elemental velocities, $\mathbf{S}_{vv}$, due to the road excitation can be expressed, using Eq. (4), in terms of the spectral density matrix of road displacement, $\mathbf{S}_{dd}$ in Eq. (5), as

$$\mathbf{S}_{vv} = \mathbf{T}\mathbf{S}_{dd}\mathbf{T}^{\mathrm{H}}. \tag{6}$$

Eq. (6) demonstrates the simplicity of the proposed analysis method, i.e. it is possible to express in just one equation the relationship between road profile and tyre vibration. As shown in the following sections, the force transmitted to the hub from the tyre can also be calculated using this approach, as well as the noise radiated by the tyre and the structure-borne sound inside the vehicle.

3. Modelling of the problem

3.1. The tyre model

The tyre used as an example in this work is an experimental prototype tyre built by Goodyear for the fourth frame work European research contract Ratin [17]. It is a slick tyre, quite similar in build to the commercial tyre Goodyear NCT5. Based on the geometry and the properties of the many fabrics and steel layers and the various rubber compounds, a condensation procedure was used to formulate a conventional finite element (FE) model. This model employs some 300,000 degrees of freedom for the structure, with additional degrees for the contained fluid. The side walls and the tyre belt were described by anisotropic deep shell elements while the rubber layer on top of the belt, the tread, was modelled by isotropic solid elements. The tyre geometry and the state of pre stress were determined by a nonlinear numerical procedure where the tyre gradually was inflated to 2 bar.

There are a number of shortcomings with this conventional approach. The standard procedure for fluid structure interaction in commercial FE software involves a modal superposition technique where the fluid and structure modes are determined separately. Using such modal procedures, it is difficult to attribute damping at different locations that also varies depending on what strain degrees are engaged in the deformation. The viscoelastic characteristics influence the forced response of tyres greatly and therefore a direct approach would be preferable. To overcome these limitations, a direct solution technique was developed, which is based on a waveguide FE formulation [18–20].

The waveguide Finite Element Method (FEM) is useful for structures, e.g., smooth car tyres, which have constant cross sectional material and geometrical properties along one coordinate direction. In fact, for such a structure, a variable of response, say u, can be described on the following form:

$$u(x, y, \phi) = \mathbf{\Psi}(x, y)^{\mathrm{T}}\mathbf{v}(\phi, \omega), \tag{7}$$

where x, y are coordinates on the cross section, ϕ measures the angle around the structure, $\mathbf{\Psi}$ is a vector of polynomial FE shape functions, each non-zero within one FE only, and the entries of the vector $\mathbf{v}$ are the nodal displacements. A harmonic time dependence on the form $e^{j\omega t}$ is assumed and suppressed.

The structural elements used in Eq. (7) are described in Ref. [19], while the fluid elements and the fluid–structure coupling elements are defined in Ref. [18]. The structural elements include the pre-stress and the anisotropic material data as specified by the original FE model. However, instead of the linear elements,

quadratic interpolation is used. Three different tyre meshes were originally developed from the original FE mesh but the elements have been enriched by an additional node along each edge. The medium mesh is a similar but reduced mesh while the coarse mesh is further reduced. For each element, stiffness and mass properties, which are different for each element, are defined by the original FE model, suitably averaged for the coarser meshes.

Convergence studies show that the results from the medium mesh close matches those of the full mesh for the frequency range where the belt can be described as a deep shell, which is approximately up to 1.5 kHz [21–23]. The coarse mesh performs well up to approximately 400 Hz. Here, the focus is on a lower frequency range and the prime concern is not on tyre modelling but to demonstrate a full calculation scheme for tyre noise prediction; therefore the coarse mesh has been adopted. This mesh is shown in Fig. 3. Each cross section has 15 deep shell elements, for the side wall and belt, 5 solid elements, for the tread, and 47 fluid elements for a total of 353 degrees and thus, for a conventional FE model with 64 cross sections, there would be 22,592 degrees in total.

To determine appropriate losses an experimental modal analysis was used and the dynamic shear modulus of a tread sample was measured. The observed losses were then distributed in the structure and for the different components of strain, based on an ad hoc optimisation procedure [21]. Based on this procedure, the tread has a frequency independent loss factor of 0.25, which is the value measured at 250 Hz, while the loss factor for the air contained in the tyre was only 0.0025. The deep shell elements have different loss factors for different kinds of strain, which varies in between 0.2 for crosswise bending to 0.01 for circumferential in-plane strain.

The element formulations are built upon a variant of Hamilton's principle, which is valid for dissipative motion [19,20,24,25]. Displacement fields of the form in Eq. (7) are assumed. Then, standard FE procedures for element evaluation and assembling are applied and the following Lagrange-Euler equation for the tyre follows:

$$\left[\mathbf{K}_2\frac{\partial^2}{\partial\phi^2}+\mathbf{K}_1\frac{\partial}{\partial\phi}+\mathbf{K}_0-\mathrm{j}\omega\mathbf{G}-\omega^2\mathbf{M}\right]\mathbf{v}(\phi,\omega)=\mathbf{f}(\phi,\omega), \tag{8}$$

where $\mathbf{f}$ is the corresponding generalised force vector, the matrices $\mathbf{K}_2$, $\mathbf{K}_1$, $\mathbf{K}_0$ and $\mathbf{M}$ describe the elastic and inertia forces of the structure and the fluid while the matrix $\mathbf{G}$ describes the fluid–structure coupling. Non-proportional damping is attributed by the imaginary parts of the matrices $\mathbf{K}_2$, $\mathbf{K}_1$ and $\mathbf{K}_0$.

In the absence of external forces, Eq. (8) is a wave equation, describing propagation around the tyre. Such equation is a set of coupled ordinary differential equations with constant coefficients and hence the solutions

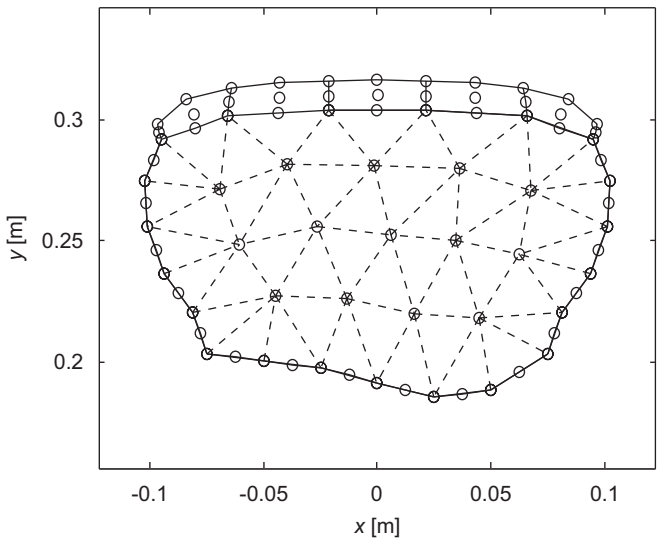

Fig. 3. Mesh used in the waveguide FE model of the car tyre. Circles indicate node locations.

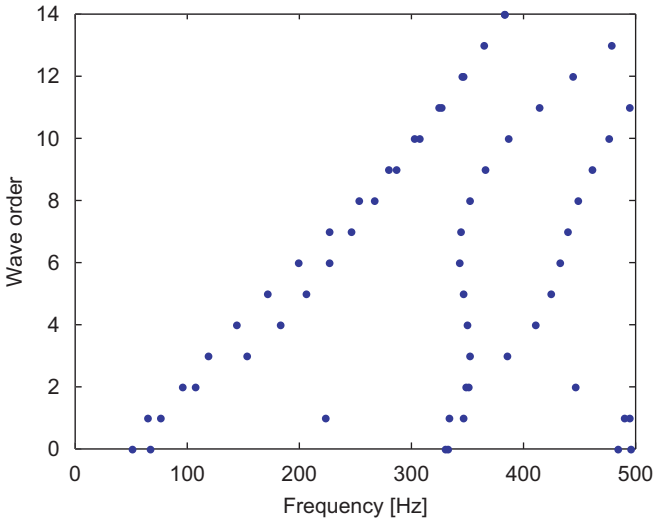

Fig. 4. Dispersion relations where each dot corresponds to a natural mode.

are exponential functions of the form

$$\mathbf{v}(\phi,\omega)=\mathbf{\Theta}(\omega)\mathrm{e}^{-\mathrm{j}k\phi}. \tag{9}$$

Using this assumption, the wave equation becomes a polynomial eigenvalue problem, relating the eigenvalue, the wavenumber k, to a given frequency ω, or vice versa. Each of these eigensolutions describe a wave that either propagates or decays around the tyre and to each solution there is a corresponding wave form [18,20,21].

Fig. 4 shows the dispersion relations for the tyre, that is the number of wavelengths around it as function of frequency. In the dispersion curve each dot corresponds to a natural mode. The first two branches from the left correspond to the symmetric and anti-symmetric belt modes while the third and fourth branches are the symmetric and anti-symmetric belt bending modes. The two isolated dots at about 225 and 450 Hz are the first two fluid modes.

The tyre is a circular structure and therefore the forced response solutions are periodic functions of ϕ. Hence, they can be expressed by an exponential Fourier series,

$$\mathbf{v}(\phi,\omega)=\sum_n \tilde{\mathbf{v}}_n(\omega)\mathrm{e}^{\mathrm{j}n\phi} \tag{10}$$

and similarly for the force vector. It follows that $\mathbf{v}$ is given by the solutions to

$$\mathbf{D}_n(\omega)\tilde{\mathbf{v}}_n(\omega)=\tilde{\mathbf{f}}_n(\omega), \tag{11}$$

where $\mathbf{D}_n(\omega)$ is given by the matrices on the left-hand side of Eq. (8).

Fig. 5 shows the predicted response of a freely suspended tyre, to a radial point excitation at the middle of the cross section. This is in good agreement with measurements [21,22]. The visible peaks between 70 and 250 Hz are modes where the belt move rigidly above the side wall. The first peak involves also an anti-symmetric rigid belt mode that is excited because the rim is not symmetric about the middle of the tyre cross section. This peak is somewhat broader than the others and, in the measurement, the following anti-resonance is less pronounced. The acoustic mode around 225 Hz is just about visible in the sixth peak. The broad peak around 350 Hz consists of the first eight, or so, belt symmetric bending modes.

3.2. The road excitation

The road roughness is a random variable whose properties vary with the type of road surface, as described by Robson [26]. The time varying road displacement $d(t)$ is derived from traversing, at velocity v, a rigid road

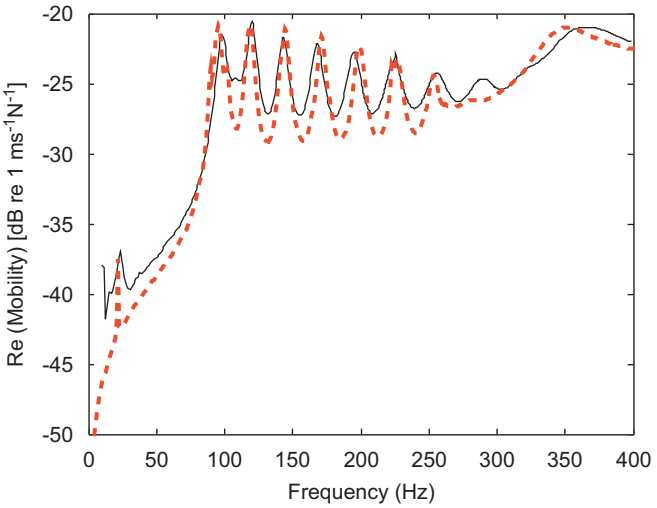

Fig. 5. Real part of point mobility of a freely hung tyre. Solid black line, measured [18]; dashed red line predicted.

profile. The excitation spectral density $S_d(f)$ at a contact point can be modelled for any particular vehicle velocity as

$$S_d(f) = \frac{c}{v}\left(\frac{f}{v}\right)^{-2.5}, \tag{12}$$

where f is the excitation frequency and c is a constant given in Ref. [26]. The ISO 8608 standard [27] also suggests using a similar description of the road profile. Moreover, Robson [26] discusses experimental evidence for the roughness being approximately homogeneous and isotropic and he proposes a two-dimension Gaussian model to represent a road surface.

By assuming the road roughness possesses the property of isotropy [26,28] it is possible to base a 2D spectral surface on the previously established single-profile spectrum. In fact the cross correlation R_{ab} between two parallel profiles a and b can be found simply adopting the isotropy property, i.e. all profiles, irrespective of orientation and location, have the same spectral density. It follows:

$$\begin{aligned} R_{ab}(\delta) &= E[z_a(x)z_b(x+\delta)] \\ &= E[z_a(x)z_a(x+\sqrt{\delta^2+\varepsilon^2})] = R_{aa}(\sqrt{\delta^2+\varepsilon^2}), \end{aligned} \tag{13}$$

where ε is the distance between the two profiles. Eq. (13) gives the relationship between the cross-correlation of two parallel profiles and the auto-correlation of the profile.

In the spatial domain, the relationship between the single-sided spectral density $G(n)$ and the autocorrelation function $R(\delta)$, reminding they are real function, are given by [29,30]

$$G(n) = 4\int_0^\infty R(\delta)\cos(2\pi n\delta)\,\mathrm{d}\delta \tag{14}$$

and

$$R(\delta) = \int_0^\infty G(n)\cos(2\pi n\delta)\,\mathrm{d}n, \tag{15}$$

where δ is distance and n is the wavenumber expressed in cycles per unit length.

In order to evaluate these integrals, $G(n)$ must be specified at all wavenumbers $|n|<\infty$, whatever the range of interest. These only converge, however, for profile descriptions $G(n)$ which satisfy admissibility criteria

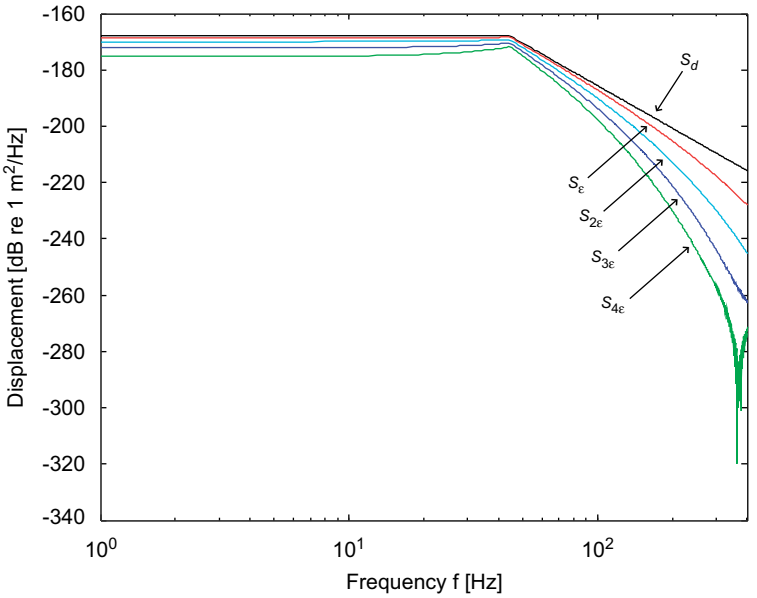

Fig. 6. Road auto-spectral density S_d and cross-spectral densities at distances of ε, 2ε, 3ε and 4ε for a road velocity of 80 km/h, with $\varepsilon = 2.15$ cm.

given in [28]. The most convenient acceptable profile description is

$$G(n) = \begin{cases} cn_a^{-2.5}, & 0 < |n| < n_a, \\ cn^{-2.5}, & n_a < |n| < n_b, \\ 0, & n_b < |n|, \end{cases} \tag{16}$$

where n_a and n_b are constants and c has the value suggested in Ref. [26]. The results presented here refers to $n_a = 2$ and $n_b = 70$ cycles m^{-1}. The wavenumber $n_b = 70$ cycles m^{-1} has been chosen in order to excite all the frequencies in the range of interest. In fact n_b is related to a frequency of 400 Hz for the lower tyre speed of 20 km/h. On the contrary, n_a has been chosen so that the lower excitation frequency was smaller then the first natural frequency of the tyre. In the frequency range of interest, i.e. 10–400 Hz, and considering a range of velocities between 20 and 100 km/h, a road roughness valid for wavelength between 14 and 3 m is ideally required. However, the tyre elements in the contact area have a width of 31 mm in the circumferential direction, so the model can be considered reliable only down to excitation wavelength of about 62 mm ($n_a = 17$ cycles m^{-1}) in order to avoid geometric aliasing. As a consequence, because of the geometrical aliasing, the maximum frequency of the excitation is limited to 100 Hz for the lower tyre speed of 20 km/h. Although the roughness road spectral description using Eq. (12) was originally proposed in Ref. [26] for a wavelength range up to two order of magnitude, the model has been extended to cover the wavelengths range of interest here [31,32].

Fig. 6 shows the auto-spectral density S_d of the road-profile at a velocity of 80 km/h for a value of the constant c of 50×10^{-8}. This road spectrum has been used for all the numerical calculation presented in the paper. In the same figure the magnitude of the cross-spectral density between parallel profiles are shown for the same velocity and at distances between the profiles of ε, 2ε, 3ε and 4ε. The distance ε between two profiles has been set to $\varepsilon = 2.15$ cm, that is the axial distance between tyre nodes in the contact patch. A global property, that gives an indication of the road roughness, is the rms value of the road profile. Such a quantity can be calculated from Eq. (16) as

$$\mathrm{rms}(G) = \sqrt{c\left(\frac{5}{3}n_a^{-1.5} - \frac{2}{3}n_b^{-1.5}\right)}. \tag{17}$$

The road profile used in the simulations has an rms value of 0.5 mm.

4. Numerical results

In order to carry out the numerical simulation some further parameters of the model have to be set. The value of the spring stiffness in the contact area, k_i, has been found by assuming a value of the bedding global stiffness of $160\,\mathrm{KN\,m^{-1}}$ as suggested by Lasson [15] and confirmed experimentally by Gäbel and Kröger [33]. It is difficult to define the stiffness of the individual spring in order to give a realistic description of the elastic properties of the tread surface, and moreover, the contact stiffness depends on the specific tyre being modelled and the roughness of the road surface [15]. However, as will be shown below, the overall model gives reasonable predictions of tread velocity and force transmission. The contact patch has been fixed so that $N_c = 15$, with 3 radial and 5 axial elements. The contact patch length is then 10 cm, which is congruent with the experimental value measured in Ref. [34]. Such results have been confirmed also by an analysis of the static deformation of the tyre model using contact penalty functions [32] subjected to the weight of a car quarter.

Moreover, a full tyre mesh (see Fig. 2) has been obtained from the tyre section mesh (see Fig. 3) taking into account only the 31 external nodes and copying such a section into 64 circumferential sections, for a total of $N_T = 1984$.

4.1. Evaluation of the tyre vibration

The spectral density matrix of the tyre's velocities can be calculated using Eq. (6), in which the diagonal terms represent the auto-spectral densities of each elements velocity. Using these auto-spectral densities, it is then possible to evaluate the rms velocity of each elements. Fig. 7 shows the rms velocity of each of the elements of the tyre when the road is travelling under the tyre at a velocity of 80 km/h. The assumed road roughness spectrum at this velocity is shown in Fig. 6. In order to represent the results most clearly, the tyre has been flattened, keeping the contact area at the centre of the figure. The circles show the contact points, that is the points where the road excitation has been applied. The boundary between tread and sidewall occurs at about ±0.1 m from the wheel centre. As expected, the tyre velocity in the contact patch is much larger than for the rest of the tyre, and the velocity falls off rapidly away from the contact patch, because of the high damping of the rubber material. A main contribution to the rms tyre velocity is given by tyre's first mode, i.e. the rigid movement of the belt over the sidewall. The rms velocity of the sidewall is limited because it is constrained on one side by the hub.

Previous measurements of the accelerations of an element on the tyre surface, during its rotation against the ground, can be found in the literature [9,34]. It is shown that the acceleration of a point inside the contact patch can easily be very large. However, the average velocity perpendicular to the tyre surface, of an element outside the contact area was found to be about $1\,\mathrm{mm\,s^{-1}}$, which is consistent with these predictions.

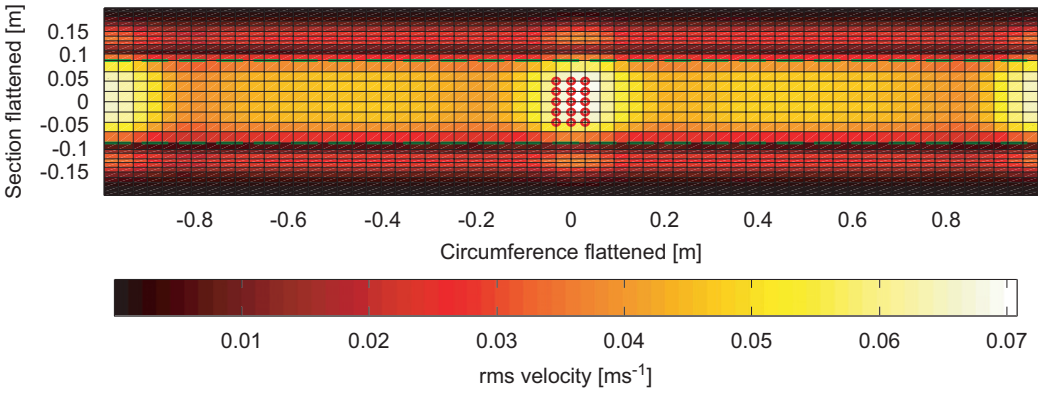

Fig. 7. rms Velocity of the tyre elements at 80 km/h. Note that distances ±0.1 m in the radial direction correspond to the tread section of the tyre and from ±0.1 to ±0.2 m to the sidewalls.

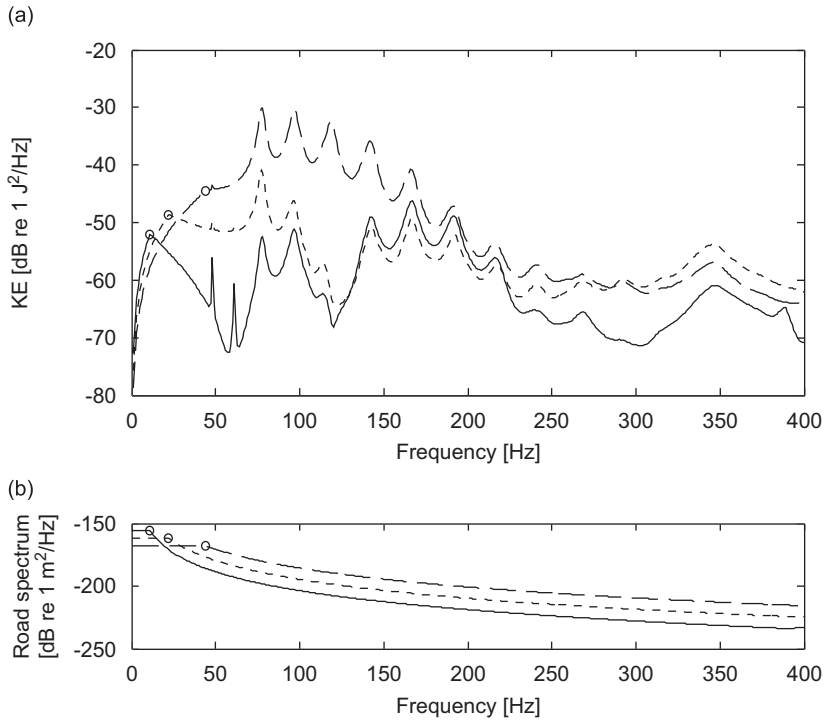

Fig. 8. Expected value of the tyre kinetic energy (a) due to the road excitation (b) at 20 (continuous line), 40 (dotted line) and 80 (dashed line) km/h.

The kinetic energy associated with the radial motion of the tyre is proportional to the inner product of the vector of velocities weighted by the mass matrix $\mathbf{M}$. The expectation of tyre's radial kinetic energy E_k can be expressed as

$$E_k = \text{trace}[\tfrac{1}{4}\mathbf{M}\mathbf{S}_{vv}], \tag{18}$$

where the trace and expectation operators can be swapped since E_k is a scalar. To obtain Eq. (18) has been used the fact that the inner product of a generic vector $\mathbf{y}$ by himself is equal to the trace of the outer product of the same vector [16], $\mathbf{y}^{\mathrm{H}}\mathbf{y} = \text{trace}(\mathbf{y}\mathbf{y}^{\mathrm{H}})$.

Fig. 8(a) shows the calculated kinetic energy of the tyre evaluated at a car speed of 20, 40 and 80 km/h. The behaviour up to the circled point is due to the flat curve of the road profile spectral density, introduced in Eq. (16) and shown in Fig. 8(b). The kinetic energy does not rise monotonically with speed at all frequencies, particularly above 300 Hz. The resonant frequencies of the tyre from 80 Hz up to about 250 Hz stand clearly out. The peaks fall off with a 20 dB/decade slope at 80 km/h. At about 350 Hz we note the first bending mode across the tyre section, as shown in the dispersion curve in Fig. 4.

4.2. Evaluation of the tyre radiated sound

Once the radial velocities at each element have been specified, the complex sound pressure at any point on the surface of the tyre can be calculated using a set of acoustic radiation impedances. It is assumed that these acoustic pressures at the surface of the tyre generate a far lower response than the force vector, $\mathbf{f}_T$, and so the sound radiation can be calculated from a weakly coupled analysis. The power spectral matrix of the radiated sound pressure $\mathbf{S}_{pp}$ is then given by

$$\mathbf{S}_{pp} = \mathbf{Z}_A \mathbf{S}_{vv} \mathbf{Z}_A^{\mathrm{H}}, \tag{19}$$

where $\mathbf{Z}_A$ is the square specific acoustic radiation resistance matrix which relates $\mathbf{v}$ and the vector of surface pressures $\mathbf{p}$. The intensity of sound radiated by a structure divided into elements, each vibrating with a velocity

given by an element of $\mathbf{v}_T$, is given by

$$I_s = \tfrac{1}{2}\mathrm{Re}(\mathbf{v}_T^{\mathrm{H}}\mathbf{Z}_A\mathbf{v}_T). \tag{20}$$

Taking the expectation of Eq. (20) and using the properties of the trace operator, the radiated sound intensity can be expressed in terms of the velocity spectral density matrix as

$$I_s = \mathrm{trace}[\tfrac{1}{2}\mathbf{R}_A\mathbf{S}_{vv}], \tag{21}$$

where $\mathbf{R}_A$ is $\mathrm{Re}(\mathbf{Z}_A)$.

This acoustic matrix $\mathbf{Z}_A$ can, in principle, be measured as discussed by Koopman and Farelane [35] or calculated for a given geometry of structure, radiating into a particular environment. In this case, such a matrix has been obtained using a boundary element method (BEM) model.

The radiation model includes the tyre, the hub and the road. The same mesh used for the mechanical tyre model has been used. As a general guideline, the maximal element dimension is about 1/6 of the smallest wavelength of the radiated sound then the actual mesh is detailed enough for calculation up to 1800 Hz. Moreover, 466 nodes have been added to the tyre mesh in order to model the hub. The hub model consists of two flat rigid circles that close the hole in the tyre mesh. The tyre has been modelled in the deformed shape, due to the static load of a quarter of the car, computed using the FEM tyre model with contact penalty functions [32]. However, the spectral density matrix $\mathbf{S}_{vv}$ has been computed ignoring the changes in the tyre symmetry due to the flattening. The road has been modelled as a partial reflective plane using the mirror source method, i.e. the mesh was mirrored to the plane of the ground positioned below the tyre with a certain gap. For numerical convergence and stability reasons the solution near close parts of distinct domains gets more uncertain if the gap between the parts gets comparable with the dimensions of the elements near the gap. Therefore a minimum gap of 1 cm has been chosen. The acoustic impedance of a dense pavement has been calculated using the microstructural model, proposed by Bérengier et al. [36] for porous pavement, and modifying the model parameters in order to get an absorption coefficient between 0 and 0.06, that are the common values for dense road pavement [37,38]. The radiation impedance matrix was calculated from 1 Hz up to 300 Hz.

Fig. 9 shows the sound pressure level (SPL) at the surface of each tyre element at 80 km/h. The pressure is greatly enhanced by the reflective plane and the parts of the tyre closest to the plane have the highest pressures.

Fig. 10 shows the overall power spectrum of the radiated sound intensity of the tyre at 20, 40 and 80 km/h. These intensity levels are reasonably consistent with measured near-field pressure levels, such as Ref. [7]. The same peaks and a similar shape is seen in this spectrum and that for the kinetic energy (Fig. 8(a)). This method of analysing the radiated sound intensity would permit the relationship between the road characteristics and the tyre acoustic emission to be further explored.

These results refer to a tyre shape deformed by the static weight of a quarter car and to a surface with the sound absorption properties of a dense pavement. It has been seen that considering the undeformed shape of the tyre and a fully reflective surface do not change significantly the sound radiation results. In fact the sound absorption coefficient of a dense pavement is very low and it can be neglected. Instead, in the case of porous pavements, the sound absorption coefficient needs to be accounted for.

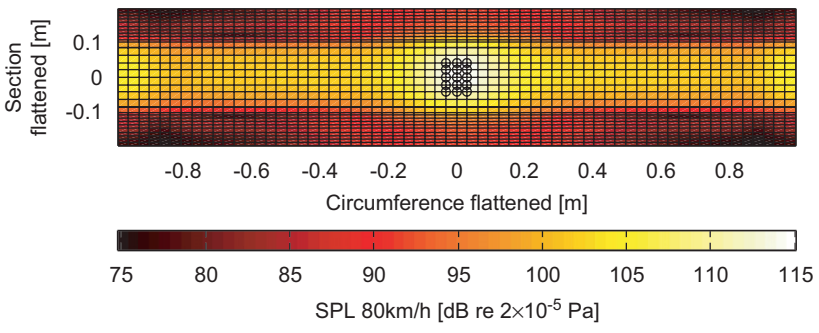

Fig. 9. The sound pressure level (SPL) calculated at the surface of the tyre elements at 80 km/h.

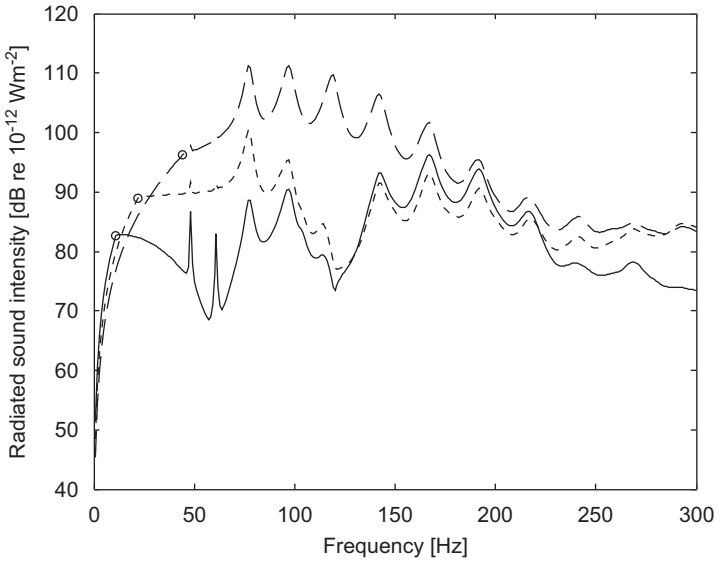

Fig. 10. Radiated sound intensity at 20 (continuous line), 40 (dotted line) and 80 (dashed line) km/h.

4.3. Evaluation of the generated interior noise

The internal sound field in the vehicle is assumed to be entirely structure-borne, and to be excited by the vibration of the tyre hub, which seems reasonable in the low-frequency range where the model has to be applied [4]. The hub has been considered as a rigid body to which five force components are applied from the tyre and through the tyre. These components correspond to three linear forces and two moments. In fact, the moment around the tyre axis can be neglected since due only to the bearing's friction. These complex forces can be represented as the elements of the vector $\mathbf{f}_H$, and are assumed to be generated by the vibration of the road, $\mathbf{d}$. The linear transformation from the road excitation to the hub forces, which is governed by the tyre's dynamics, is represented by

$$\mathbf{f}_H = \mathbf{Z}_{HT}\mathbf{Z}_{TC}\mathbf{d}, \tag{22}$$

where $\mathbf{Z}_{HT}$ represents the transfer function between the force applied at the tyre $\mathbf{f}_T$ and the force at the hub $\mathbf{f}_H$, while $\mathbf{Z}_{TC}$ represents the transfer function between the road excitation $\mathbf{d}$ and $\mathbf{f}_T$. The matrix $\mathbf{Z}_{HT}$ has been obtained from the tyre waveguide FEM model while the matrix $\mathbf{Z}_{TC}$ can be found from Eqs. (2) and (3) to be

$$\mathbf{Z}_{TC} = [\mathbf{I} + \mathbf{K}_{TC}\mathbf{C}_{CT}]^{-1}\mathbf{K}_{TC}. \tag{23}$$

The acoustic pressures at a set of points inside the vehicle are represented as the complex elements of the vector $\mathbf{p}_I$. These are assumed to be generated by the hub forces, $\mathbf{f}_H$, by a matrix of complex impedances, $\mathbf{Z}^h_{IH}$, that represent both the structural response of the vehicle and the acoustic response of its interior. The internal pressures are thus given by

$$\mathbf{p}_I = \mathbf{Z}^h_{IH}\mathbf{f}_H, \tag{24}$$

where $h = 1, 2, 3, 4$ is the index of the four hubs in the car.

The impedance matrices $\mathbf{Z}^h_{IH}$ have been computed by means of a numerical trimmed model of a small class car. Both the solid structure and the fluid cavity have been modelled. The vehicle trimmed body FE model (see Fig. 11(a)) consisted of the complete vehicle without powertrain and exhaust system. The structural metal parts of the vehicle have been modelled with shell elements with an average size to correctly simulate the mode shapes of the whole vehicle up to 200 Hz. As a result, the number of shell elements is usually larger than 3 million degrees of freedom. The structure also includes an FEM model of the suspensions. Typical characteristics of bushings and dampers have been linearised about the standard static configuration assuming

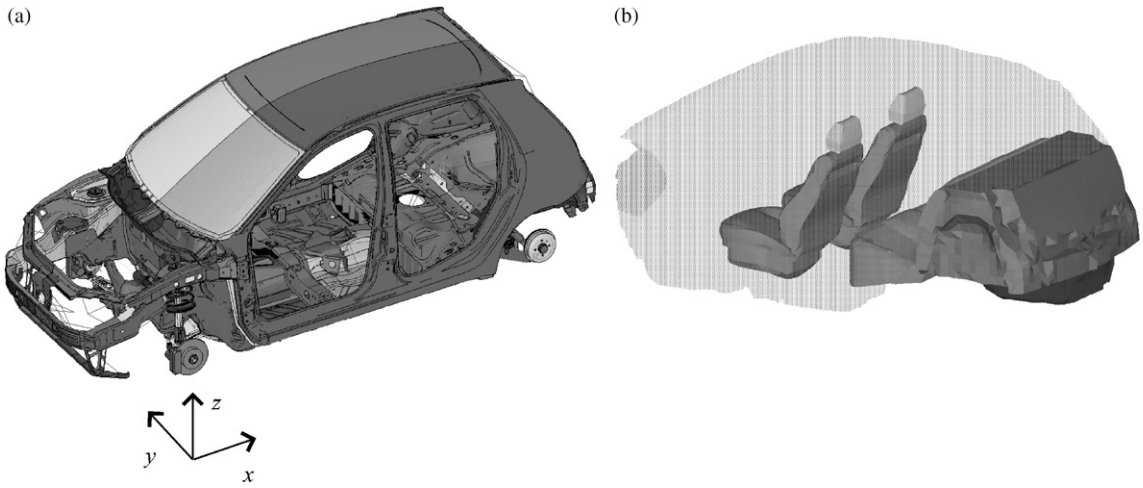

Fig. 11. Structural (a) and internal cavity (b) models.

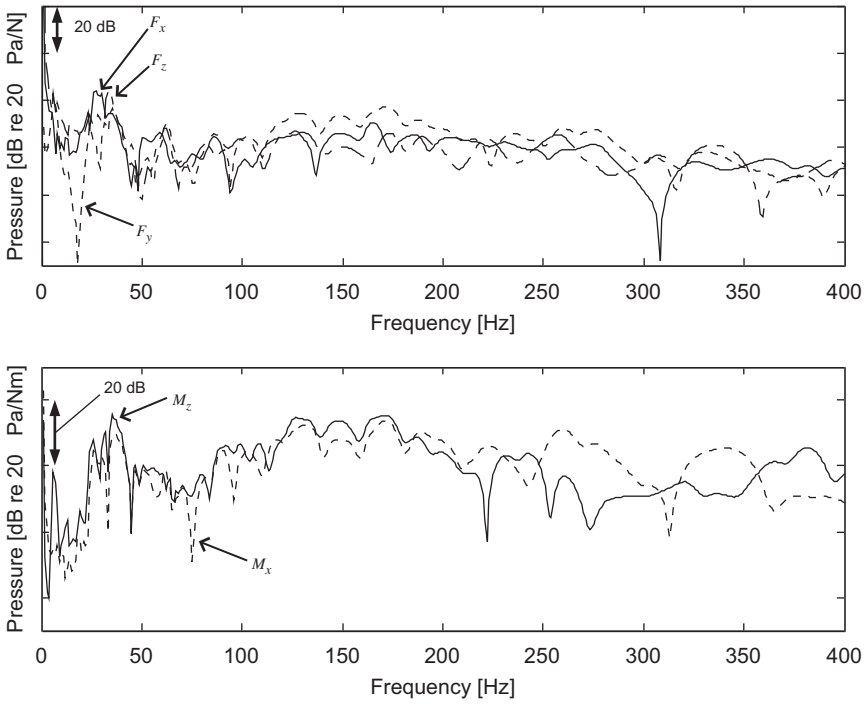

Fig. 12. Pressure at the driver's left ear (in a left-hand drive car) when the left front wheel is excited with forces F_x, F_y and F_z, of 1 N, (above) or moments M_x and M_z, of 1 Nm, (below) applied on different directions.

that, for all the loads on the car, the dynamic forces are within the range of linearisation. With this approximation is possible to estimate the correct behaviour of the dynamic stiffness of the bushing up to 90 km/h. The internal cavity has been modelled with brick elements as shown in Fig. 11(b). The model includes the seats and the trunk compartment. The two sub-models have been connected by means of a fluid structure interaction (FSI) technique [39,40]. The model has also been validated up to 200 Hz, and so the results above this frequency are not reliable.

Fig. 12 shows the predicted pressure at the driver's left ear (in a left-hand drive car) when the left front wheel is excited with unitary forces and moments on different directions. The curves show that the y direction, as indicated in Fig. 11(a), is the most sensitive to the forces applied to the hub only in the frequency range 100–200 Hz even though the suspension is stiff in that direction since it has to counteract the external forces during cornering.

The response of the tyre in Eq. (22) can be combined with the response of the vehicle in Eq. (24) to give the internal pressures as a function of the road displacement

$$\mathbf{p}_I = \mathbf{Z}_{IT}\mathbf{d}, \tag{25}$$

where

$$\mathbf{Z}_{IT} = \left[\sum_{h=1}^{4} \mathbf{Z}_{IH}^{h}\right] \mathbf{Z}_{HT}\mathbf{Z}_{TC} \tag{26}$$

and each tyre has been supposed to be excited by the same road displacement $\mathbf{d}$.

The matrix $\mathbf{Z}_{IT}$ could incorporate the effects of a compliant connection from the vehicles suspension system at the wheel hub, but for simplicity this connection is assumed here to be rigid. This simplification is supported by the fact that the car impedance at the hub is much greater than the tyre impedance so that car and tyre systems can been considered separately. In particular the tyre has been considered grounded at the hub while the car has been considered free at the hubs when the excitation has been applied.

A useful representation of the average acoustic pressure inside the vehicle is the sum of the squared pressures at a set of points. A set of eight points inside the car cavity has been considered. The points have been placed at the average position of the passengers and driver ears. The main point of application of forces are the four wheel hubs. Using Eq. (25) and the properties of the trace operation, the sum of square pressures can be represented as a function of the spectral density matrix of the road excitation, $\mathbf{S}_{dd}$, as

$$P_i = \mathrm{trace}[\mathbf{Z}_{IT}\mathbf{S}_{dd}\mathbf{Z}_{IT}^{\mathrm{H}}]. \tag{27}$$

Fig. 13 shows the predicted sum of the squared pressures P_i as A-weighted SPL at the eight earing points inside the car cavity when the car is travelling at a velocity of 20, 40 and 80 km/h. The peaks at 58.7 and 98.1 Hz correspond to the first two internal air cavity resonance of the car. The evident peak at about 225 Hz could be related to the first tyre fluid mode which is shown in Fig. 4. Integrating the sound pressure spectrum over the full frequency range a SPL of 63, 77 and 86 dB(A) has been obtained for the road velocity of 20, 40

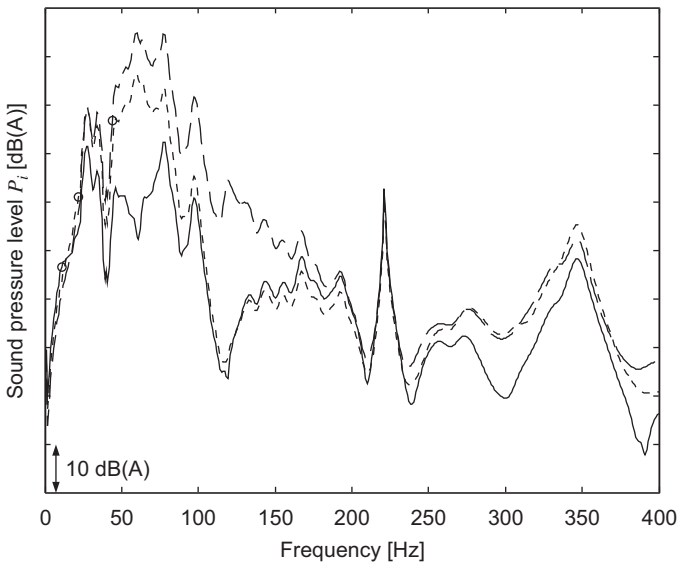

Fig. 13. Sound pressure level at the 8 passenger ears at 20 (continuous line), 40 (dotted line) and 80 (dashed line) km/h.

and 80 km/h. Such results are sufficiently in good approximation to the structure borne noise measured by Jha [4].

5. Conclusions

In this paper, a full linear model has been applied to a 3D tyre model and its road excitation. The contact of the tyre with the ground has been modelled by a Winkler model and the road excitation has been expressed by the spectral distribution of a common road surface. The tyre has been modelled by a waveguide FEM and a BEM calculation has been used to find the radiation tyre matrix. Hence the tyre vibratory level and its radiated sound have been computed. Moreover, a FEM model of a commercial car has been considered in order to compute the noise level inside the car.

The linear model introduced to describe the tyre excitation due to the road interaction has resulted in a computationally efficient method of predicting the tyre vibration level, much quicker than traditional nonlinear approaches. Moreover such model permits to calculate the noise radiated by the tyre and the car interior noise in a straightforward way. It thus appears to be a useful tool for the rapid evaluation of the noise generation into a vehicle and then suitable to industrial design applications.

An examination of the effects of the nonlinearity in the contact patch and the tyre tread pattern, and their potential incorporation into the stochastic road excitation model remain as further work, as does a more complete experimental validation of the method.

Acknowledgements

This work is supported by the EU under the integrated project "Integrated materials for active noise reduction", InMAR. The car frame data have been used by courtesy of FIAT Auto.

References

[1] U. Sandberg, Tyre/road noise—myths and realities, *Proceeding of Inter-Noise 2001*, 2001, pp. 35–56.
[2] U. Sandberg, G. Descornet, Road surface influence on tyre/road noise—part 1, *Proceeding of Inter-Noise 80*, Vol. 1, 1980, pp. 259–266.
[3] F. Anfosso-Lédée, M.-T. Do, Geometric descriptors of road surface texture in relation to tire-road noise, *Transportation Research Record* 1806 (02-2958) (2002) 160–167.
[4] S. Jha, Identification of road/tyre induced noise transmission paths in a vehicle, *International Journal of Vehicle Design* 5 (1/2) (1984) 143–158.
[5] G.J. Kim, K.R. Holland, N. Lalor, Identification of the airborne component of tyre-induced vehicle interior noise, *Applied Acoustics* 51 (2) (1997) 141–156.
[6] A. Kuijpers, G. van Blokland, Tyre/road noise models in the last two decades: a critical evaluation, *Internoise 2001*, The Hague, The Netherlands, 2001, pp. 2593–2598.
[7] J. Haberl, J. Litzka, Near-field noise emissions on austrian road surface courses, *Euronoise 2006*, Tampere, Finland, 2006, Paper 19.
[8] W. Kropp, F.-X. Bécot, S. Barrelet, On the sound radiation from tyres, *Acustica* 86 (2000) 760–779.
[9] F. Wullens, W. Kropp, A three-dimensional contact model for tyre/road interaction in rolling conditions, *Acta Acustica united with Acustica* 90 (2004) 702–711.
[10] S. Fong, Tyre induced predictions from computed road surface texture induced contact pressure, *Internoise 98*, Christchurch, New Zealand, 1998.
[11] E. Rustighi, S.J. Elliott, M.A. Sek, Stochastic analysis of the non-linear road/tyre excitation, *Euronoise 2006 6th European Conference on Noise Control, Vol. Supplement 1 of Acta Acustica United With Acustica, European Acoustic Association* (EAA), S. Hirzel, Tampere, Finland, 2006, p. S 74, not Refereed.
[12] E. Rustighi, S. J. Elliott, A model of tyre vibration with stochastic excitation, *ICSV12 Twelfth International Congress on Sound and Vibration*, Lisbon Portugal, 2005, cDRom.
[13] E. Rustighi, S.J. Elliott, Stochastic road excitation and control feasibility in a 2d linear tyre model, *Journal of Sound and Vibration* 300 (3–5) (2007) 490–501.
[14] K. Johnson, *Contact Mechanics*, Cambridge University Press, Cambridge, 1985.
[15] K. Larsson, Modelling of Dynamic Contact—Exemplified on the Tyre/Road Interaction, PhD Thesis, Department of Applied Acoustics, Chalmers University of Technology, Göteborg, Sweden, 2002.
[16] S. Elliott, *Signal Processing for Active Control*, Academic Press, New York, 2001.

[17] A. Pietrzyk, Prediction of the dynamic response of a tire, in: R. Boone (Ed.), *Proceedings of Inter-noise 2001*, Vol. 5, The Hague, The Netherlands, 2001, pp. 2547–2550.
[18] C.-M. Nilsson, Waveguide Finite Elements Applied on a car Tyre, Doctoral Thesis, KTH Royal Institute of Technology, Department of Aeronautical and Vehicle Technology, Stockholm, 2004. Available: ⟨http://www.diva-portal.org/kth/theses/abstract.xsql?dbid=3812⟩. [Accessed 27 June 2007].
[19] S. Finnveden, Waveguide Finite Elements for Curved Structures, TRITA-AVE 2006:38, Journal of Sound and Vibration, (2006), submitted. Available: ⟨http://www.ave.kth.se/staff/mwl/Svante_Finnveden.html⟩ [Accessed 27 June 2007].
[20] C.-M. Nilsson, S. Finnveden, Input power to waveguides calculated by a finite element method, *Journal of Sound and Vibration* (2007) doi:10.1016/j.jsv.2007.04.025.
[21] M. Fraggstedt, Power Dissipation in Car Tyres, Licentiate Thesis TRITA-AVE 2006:26, MWL/KTH, 2006. Available: ⟨http://www.diva-portal.org/kth/abstract.xsql?dbid=3994⟩ [Accessed 27 June 2007].
[22] S. Finnveden, C.-M. Nilsson, M. Fraggstedt, Waveguide fea of the vibration of rolling car tyres, *Novem*, Saint Raphael, 2005.
[23] M. Fraggstedt, S. Finnveden, Rolling resistance of car tyres, *Euronoise 2006*, Tampere, Finland, 2006, Paper 185.
[24] P.M. Morse, H. Feshbach, *Methods of Theoretical Physics*, McGraw-Hill, New York, 1953 Chapter 3.
[25] S. Finnveden, Exact spectral finite element analysis of stationary vibrations in a rail way car structure, *Acta Acustica* 2 (6) (1994) 461–482.
[26] J.D. Robson, Road surface description and vehicle response, *International Journal of Vehicle Design* 1 (1) (1979) 25–35.
[27] Mechanical Vibration—Road Surface Profiles—Reporting of Measured Data, ISO 8608, 1995.
[28] K.M.A. Kamash, J.D. Robson, The application of isotropy on road surface modelling, *Journal of Sound and Vibration* 57 (1) (1978) 89–100.
[29] B.R. Davis, A.G. Thompson, Power spectral density of road profile, *Vehicle System Dynamics* 35 (6) (2001) 409–415.
[30] D.E. Newland, An Introduction to Random Vibrations, Spectral and Wavelet Analysis, third ed., Dover, 2005.
[31] U. Sandberg, Road traffic noise—the influence of the road surface and its characterization, *Applied Acoustics* 21 (1987) 97–118.
[32] P. Andersson, Modelling Interfacial Details in Tyre/Road Contact—Adhesion Forces and Non-linear Contact Stiffness, PhD Thesis, KTH, Chalmers University of Technology, Göteborg, Sweden, 2005.
[33] G. Gäbel, M. Kröger, Non-linear contact stiffness in tyre–road interaction, *Euronoise 2006*, Tampere, Finland, 2006, Paper 118.
[34] J. Périsse, A study of radial vibrations of a rolling tyre for tyre-road noise characterisation, *Mechanical Systems and Signal Processing* 16 (6) (2002) 1043–1058.
[35] G. Koopman, J. Farelane, *Designing Quiet Structures*, Academic Press, New York, 1997.
[36] M.C. Bérengier, M.R. Stinson, G.A. Daigle, J.F. Hamet, Porous road pavements: acoustical characterization and propagation effects, *Journal of the Acoustical Society of America* 101 (1) (1997) 155–162.
[37] M.J. Crocker, D. Hanson, Z. Li, R. Karjatkar, K.S. Vissamraju, Measurement of acoustical and mechanical properties of porous road surfaces and tire and road noise, *Transportation Research Record: Journal of the Transportation Research Board* 1891 (2004) 16–22.
[38] M.J. Crocker, Z. Li, J.P. Arenas, Measurements of tyre/road noise and of acoustical properties of porous road surfaces, *International Journal of Acoustics and Vibration* 10 (2) (2005) 52–60.
[39] D.J. Nefske, S.H. Sung, *Sound in small enclosures, Noise and Vibration Control*, Wiley, New York, 1992, pp. 145–174 (chapter 6).
[40] O.C. Zienkiewicz, R.L. Taylor, Coupled systems, The Finite element method, Vol. 2, *Solid and Fluid Mechanics Dynamics and Non-Linearity*, fourth ed., McGraw-Hill International, 1991, pp. 404–437 (chapter 9).